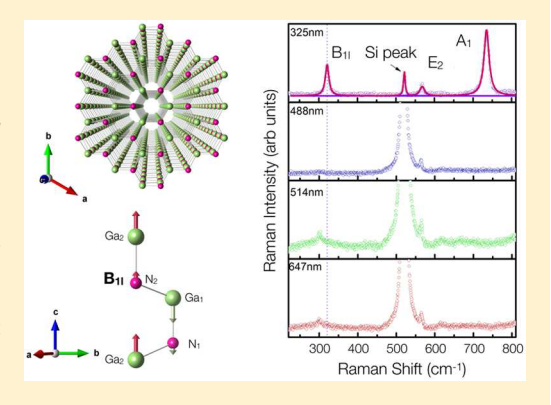
Isotopic Heft on the $B_{1/2}$ Silent Mode in Ultra-Narrow Gallium Nitride **Nanowires**

Carlos Rodríguez-Fernández, ^{†©} Mohammed Almokhtar, ^{§,†©} Wilfredo Ibarra-Hernández, ^{||,⊥©} Mauricio Morais de Lima, Jr., ^{‡©} Aldo H. Romero, ^{||,⊥©} Hajime Asahi, ^{#©} and Andrés Cantarero*, ^{†©}

Supporting Information

Downloaded via WEST VIRGINIA UNIV on August 17, 2018 at 23:20:54 (UTC). See https://pubs.acs.org/sharingguidelines for options on how to legitimately share published articles.

ABSTRACT: Wurtzite semiconductor compounds have two silent modes, B_{1l} and B_{1h} . A silent mode is a vibrational mode that carries neither a dipole moment nor Raman polarizability. Thus, they are forbidden in both infrared reflectivity and Raman spectroscopy. Astonishingly, we detected the B_{11} mode in high-quality, ultra-narrow GaN nanowires using resonant Raman scattering, although the B_{1h} was not observed, and there is no immediate explanation for this asymmetric finding. The Raman experiments were performed using several laser lines from 647 to 325 nm; the latter is a wavelength in which Raman becomes resonant. Actually, we observed the B_{1l} mode only in resonance, indicating that the appearance of this mode is related to Fröhlich electron-phonon interactions; i.e., a dipole moment emerging in the B_{1l} silent mode may not be present in the B_{1h} mode. To shed light onto the physical origin of these observations, we performed density functional theory calculations of the lattice dynamics in GaN. We



performed a careful analysis of the different physical mechanisms that allow the forbidden mode to appear to explain the physics underlying the nonzero dipole moment in the B_{1l} mode, and the reason why this dipole moment is not present in the B_{1h} mode.

KEYWORDS: Extremely narrow nanowires, crystalline perfection, Raman spectroscopy, isotopic composition, silent modes, Fröhlich electron-phonon interaction

here has been strong interest in nitride semiconductors during recent years due to the appearance of new physical phenomena and applications.¹⁻⁴ In particular, semiconductor nanostructures based on GaN and AlN and their alloys are very attractive for use in the next generation of advanced electronic and photonic nanodevices due to their potential application in short-wavelength optoelectronics and high-temperature electronics. 5-7 In particular, the quasi-one-dimensional nanostructures called nanowires (NWs) offer advantages over bulk or thin films that suffer from lattice mismatch due to a lack of a suitable substrate. The first advantage is the phenomenon called self-purification, which appears due to the diffusion or segregation of point defects to the NW surface, where they disappear during growth from the NW core.8 This phenomenon is obviously more important in thin NWs. In addition, the free surface of the NWs permits the elastic relaxation of the strain; therefore, dislocations are expected to be confined to the interface between the substrate and the NW interface.

Raman scattering is a nondestructive optical characterization technique used to study different properties of nanomaterials. 10 Information on the electronic structure can also be extracted via resonant Raman scattering (RRS), 11-15 which occurs when the electronic transitions are in the vicinity of the laser excitation energy. Under resonant conditions, the Raman spectra of polar optical phonons are dominated by the Fröhlich electron-phonon interaction, associated with the electrostatic interaction between the polar phonon and the virtual electrons present in the Raman process as an intermediate state. 13 The Fröhlich interaction is inversely proportional to the wave vector, which is close to zero in first-order Raman scattering and, in resonance, becomes dominant compared to the mechanical deformation potential (DP) electron-phonon interaction. The DP is a short-range interaction, but because the Fröhlich electron interaction depends on the electrostatic potential (it decreases slowly as 1/r), it is a long-distance interaction, and thus, is more effective when there is a perfectly aligned crystal with translational symmetry (high crystalline perfection). New features have been observed in nitride

Received: May 14, 2018 Revised: July 19, 2018 Published: July 25, 2018

[†]Molecular Science Institute and [‡]Materials Science Institute, University of Valencia, P.O. Box 22085, 46071 Valencia, Spain §Physics Department, Assiut University, Assiut 71516, Egypt

Applied Physics Department, West Virginia University, Morgantown, West Virginia 26506-6315, United States

¹Facultad de Ingeniería-BUAP, Apartado Postal J-39, Puebla 72570, Mexico

The Institute of Scientific and Industrial Research, Osaka University, 8-1 Mihoga-oka, Ibaraki, Osaka 567-0047, Japan.

nanowires in RRS experiments, some of which are not well-understood, ¹⁶ while others are clearly related to the surface (surface optical modes), such as those shown by Prasana et al., ¹⁷ or ascribable to the phonon density of states (DOS). ¹⁸

Gallium nitride, AlN, InN, and their alloys belong to the C_{60}^4 (P6₃mc) space group, with two formula units per primitive cell and all atoms occupying $C_{3\nu}$ sites. In a Raman spectrum, the phonons at the Γ point of the Brillouin Zone (BZ; zone center) are mainly observed because the wave number of the exciting light is basically zero (in the dipole approximation, it is strictly zero). Additionally, we can observe overtones in the Raman scattering spectrum, which are usually modes at the border of the BZ that can be accessed through two phonon processes (where $\kappa \approx q_1 \pm q_2$ is the wave vector of the light, and q_1 and q_1 are the wave vectors of the phonons involved in the second-order Raman process). Typically, there is a whole structure in the background of a Raman spectrum called twophonon DOS, which involves many phonons (there are also three- and four-phonon DOS, but they are negligible compared to the two-phonon DOS). Group theory, based on the symmetry operations of crystal atomic positions, tells us that, at the Γ point, the phonon modes in the wurtzite structure have the following decomposition pattern: 19

$$\Gamma = 2A_1 + 2B_1 + 2E_1 + 2E_2$$

The three acoustic modes are $A_1 + E_1$ (a one-dimensional A_1 and a two-dimensional mode E_1), while the remaining nine modes are optical. E_1 and A_1 are polar modes, i.e., they split into TO and LO, while the E_2 modes (E_{21} and E_{2h}) are nonpolar. Because the P63mc space group does not have a center of inversion, the polar modes $(E_1 \text{ and } A_1)$ are both Raman and infrared-active. The E_2 modes have a change in the Raman polarizability, but they do not carry a dipole moment; 10 thus, they are only Raman active. However, the B_1 modes are silent (neither Raman nor IR active), and they are observable by a technique termed hyper-Raman scattering (HRS), which is based on a two-photon excitation process. However, as far as we know, they have not been observed by HRS to date.²⁰ There are a few publications that claim to observe B_1 modes in some wurtzite materials, but there are several discrepancies in the Raman shifts between them. Furthermore, the reported spectra show very broad signals around or close to the predicted modes, so they more closely resemble a maximum in the DOS than a phonon at the Γ point.²¹ Nevertheless, per a review of the literature, the clearest example of an observation of the silent B₁ modes in wurtzite GaN was given by Ruf et al.²² using synchrotron radiation techniques. This observation more specifically used inelastic X-ray scattering, from which the complete phonon dispersion can be obtained (i.e., all of the modes are observable). These measurements indicate that these phonons are rather important input parameters in comparison with theoretical models. Additionally, there are discussions in the literature that the indication of a broad peak can also be related to vacancies or impurities that can fall in the region around the expected phonon frequency. In that respect, there should be a systematic dependence study of the phonon line width or even the peak position with respect to temperature, impurity density, etc.²³

In this Letter, we focused on the optical characterization of GaN NWs by Raman spectroscopy. The Raman backscattering spectra of these NWs were thoroughly studied using different laser lines excitations at room temperature (Figure 1). The Raman peaks were deconvoluted with Lorentzians to extract

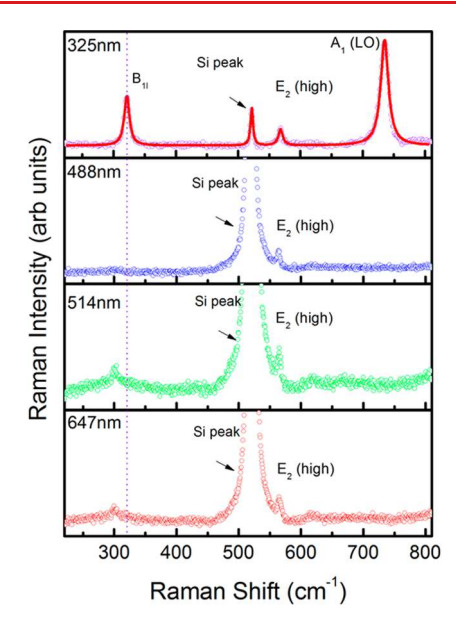


Figure 1. Raman spectra of GaN nanowires covering a wide range of interests, using for comparison the laser line excitations 325, 488, 514, and 647 nm, respectively, from top to bottom. Due to the magnification of the spectra corresponding to 647 and 514 nm (to show the presence of the E_{2h} mode), the 2TA(X) of Si (two-phonon DOS) can be clearly observed around 300 cm⁻¹.

(find the position with accuracy) the contributions from individual modes. The solid line (red online) is the cumulative fit of the Raman spectra. In back-scattering geometry with the light along the NW c axis (the NWs were grown in the wurtzite c-axis), $\overline{z}(-,-)z$ in Porto's notation, only the $A_1(LO)$ and E_2 modes are observable. The E_1 mode is observed only in the crossed-polarization geometry (also called the 90° scattering configuration).

Figure 1 shows the Raman scattering spectra measured with different laser lines (325 to 647 nm). The peak at 520.0 \pm 0.5 cm⁻¹ corresponds to the Si (substrate), which has its maximum strength at 514 nm (green). The 2TA(X) of Si, around 300 cm⁻¹, can also be observed in the spectra obtained with red and green excitation. The E_{2h} phonon mode of GaN appears at 567.1 ± 0.5 cm⁻¹, indicating that the NWs are unstressed. The reference position at which the GaN is considered unstressed is 567.5 cm⁻¹.25 The absence of stress confirms the high crystalline quality of the NWs. Only in the upper spectrum, obtained with a laser excitation of 325 nm (3.8 eV, above the GaN gap), i.e., under resonance conditions, are there two additional peaks. The first one is the $A_1(LO)$ mode located at 734.1 ± 0.5 cm⁻¹, while the second is the B_{11} mode, which is forbidden in principle but here observed due to its nonzero dipole moment and resonance effect (Fröhlich electronphonon interaction). The B_{1l} mode appears at 320.4 \pm 0.5 cm⁻¹, close to the value measured by inelastic X-ray scattering (the uncertainties in an inelastic X-ray scattering experiments are much larger than those in Raman scattering), 22 329 cm⁻¹, and our theoretical calculations at 334 cm⁻¹. The resonance conditions are demonstrated through the enhancement of the $A_1(LO)$ mode. As we know, this mode is strongly coupled to the electrons via electron-phonon Fröhlich interaction (the Fröhlich Hamiltonian is diagonal and the mode appears in parallel polarizations). Although it is possible to enhance the signal by surface enhanced Raman scattering, ^{26,27} it is better to use resonant Raman scattering if the signal is high enough

because we do not have the effect of coupling with the plasmon of the metal nanoparticle, which can give additional interactions masking the intrinsic effects. There are more measurements in the literature with an UV laser, $^{28-30}$ in GaN films, or InN/GaN core—shell NWs, but either the quality of the samples is low or the measurement range is out of the region of the B_{1l} mode. In one of them, 28 InN/GaN core—shell nanowires, the E_2 peak is far away from its position, indicating strain in the sample, producing a bad quality of the spectra.

The B_{1l} and B_{1h} mode activation is usually ascribed in the literature to a naive and uncorroborated argument: that there is a relaxation of the translational invariance due to the presence of defects, impurities, and structural disorder caused by ion implantation or mechanical damage. $^{18,23,25,31-34}$ This argument is controversial because, if there is a lack of translational invariance, the one-phonon DOS must be observed instead of the phonons at the Γ point, 35 i.e., there is some structure similar to that shown in Figure 2. Because this is not the case, the origin of the broad structures shown in refs 18, 23, 25, and $^{31-34}$ must be found in the two-phonon DOS (see the Supporting Information).

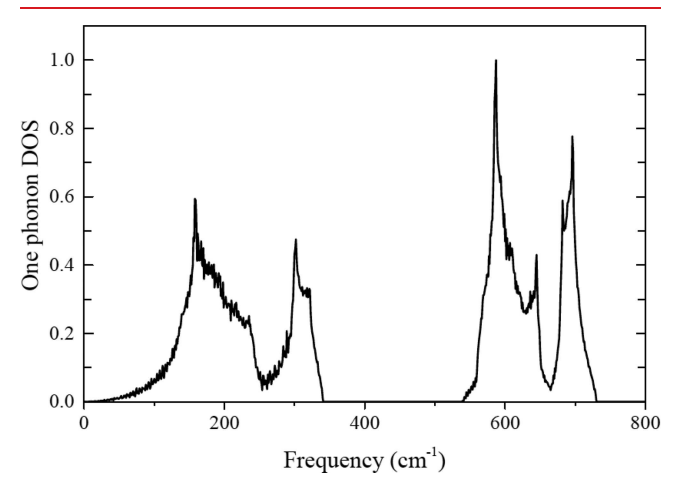


Figure 2. One-phonon density of states $(\sum_{q} \delta(\omega - \omega(q)))$. The area is normalized to the number of phonons.

In the present report, GaN NW samples with a designed diameter and length of 12 and 100 nm, respectively, were grown by plasma-assisted molecular beam epitaxy (PA-MBE) on Si(111) substrates. Reflection high-energy electron diffraction (RHEED) patterns show a reconstructed surface pattern (7×7) for the Si substrates. Elemental Ga, Al, and RF plasma-enhanced N2 were used as sources, which is a clean method for growing high-purity structures with very good crystalline quality. ^{36–39} We can exclude the existence of any phonon mode associated with lattice disorder, breakdown of the translational symmetry, or defects. The growth of the GaN NWs was performed under an N-rich condition with a Ga-to-N ratio of 1:3. The growth was started with a GaN buffer layer grown for 40 s at 450 $^{\circ}$ C, followed by thermal annealing at 800 °C for 10 min in a plasma-enhanced N₂ atmosphere to produce GaN nanoclusters. GaN NWs were grown at 800 °C for 30 min. The maximum growth rate was fixed at 200 nm/h. Although the typical growth of GaN NWs is called catalyst-free growth (we do not add a metallic nanoparticle acting as a seed) or growth of self-assembled NWs, Ga actually acts as catalyst. After the thermal annealing, the buffer layer gives rise

to a set of Ga droplets acting as catalyst, which react with the N_2 activated by the RF plasma. $^{40,41}\,$

In situ monitoring of the growing GaN NWs by RHEED patterns obtained during growth is shown in Figure 3a. The RHEED shows broken-ring patterns, indicating that hexagonal GaN NWs were grown with their c-axes (0001) perpendicular to the substrate surfaces. In addition, the X-ray diffraction (XRD) pattern image in Figure 3b was recorded using θ –2 θ scans for the structural identification. No peaks other than the diffraction peaks from GaN (0002) and Si (111) were detected, proving again that the GaN NWs were grown in the c-axis direction. High-resolution field emission scanning electron microscopy (HR-FE-SEM) and high-resolution transmission electron microscopy (HRTEM) were used for the morphological characterization of the samples (see panels c and d of Figure 3, respectively). TEM images were obtained for the GaN NWs separated from the substrate in ethyl alcohol. The SEM image clearly depicts the vertical c-oriented nanowires grown perpendicular to the SiO₂/Si substrate surfaces. Ultra-narrow GaN NWs present at a small size, with an average diameter of 12 nm and a length of 100-120 nm. The HRTEM image confirms the high-quality, singlecrystalline structure of the NWs.

Because the B_{1l} mode appears only under resonant conditions, we may attribute this mode to a Fröhlich-allowed resonant mode, although group theory indicates that this is a silent mode. The reason why this silent mode becomes Raman active due to Fröhlich electron—phonon interaction will be given below. First, we will exhaustively analyze several possible interpretations to explain the appearance of this mode in Raman experiments and why they must be excluded.

To address with some detail the observed vibrational response, theoretical calculations were performed within the framework of density functional theory (DFT)^{42,43} and density functional perturbation theory (DFPT), 44,45 as implemented in the Abinit code. 46-48 We used the generalized gradient approximation to describe the exchange-correlation energy with the Perdew-Burke-Ernzerhof (PBE) formalism. 49,50 We discretized the reciprocal space with a regular k-point mesh of $12 \times 12 \times 6$, and we selected a cutoff energy for the expansion of plane waves of 50 Ha (1360 eV). This optimization ensures that the system is fully relaxed with forces between atoms no larger than 10⁻⁴ Ha/bohr and that the stress of the crystal cell is as low as 10^{-2} GPa. For the calculation of the dynamical properties (phonons), we used DFPT with a regular q-point mesh of $4 \times 4 \times 2$. We used the *anaddb* post-processing utility provided with the Abinit code to extract the two-phonon DOS, which is a histogram of all possible phonon events with $q_1 \pm q_2$ = 0, from a Fourier-interpolated phonon grid of $40 \times 40 \times 20$. The diagonalization of the interatomic force constants also provides the eigenvectors that are analyzed within the symmetry utilities present in the Abinit code, particularly for the center-zone phonon modes.

We begin by discussing the possibility of a dipole moment appearing due to the well-known mixing between the B_1 modes. By examining the eigenvector of the B_{1h} mode, we find:

$$e_{B_{1h}} = \begin{pmatrix} +0.03951459 \\ -0.03951459 \\ -0.70600167 \\ +0.70600167 \end{pmatrix} \cong \begin{pmatrix} +0.000000000 \\ -0.000000000 \\ -0.70710678 \\ +0.70710678 \end{pmatrix}$$

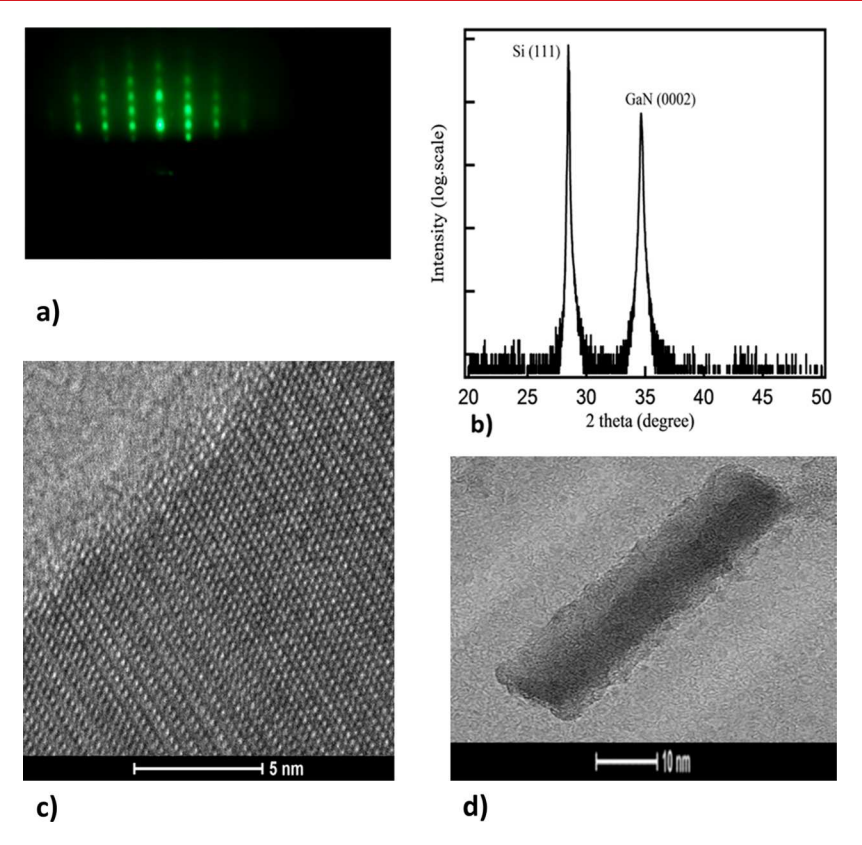


Figure 3. (a) RHEED pattern shows the c-axis growth of GaN NWs. (b) X-ray diffraction scans of the GaN NWs grown on Si(111). (c) HRTEM image showing the crystalline structure of one of the GaN NWs. (d) SEM image showing a single GaN NW grown on a Si substrate.

we realize that the value is very close to what group theory predicts. Actually, the relative displacements of Ga and N are, respectively, 0.330 and 2.642 arbitrary units (the actual values are temperature-dependent). The N planes move against each other, while the Ga planes move out of phase in comparison with other Ga planes, suppressing any possible dipole moment.

We observe a similar result for the B_{1l} mode:

$$e_{B_{11}} = \begin{pmatrix} +0.70600167 \\ -0.70600167 \\ +0.03951459 \\ -0.03951459 \end{pmatrix} \cong \begin{pmatrix} +0.70710678 \\ -0.70710678 \\ +0.00000000 \\ -0.000000000 \end{pmatrix}$$

which is also close to what group theory predicts. After accounting for the calculated eigenvectors, the relative displacements of the Ga planes are against each other, like with the N planes; however, in that case, the Ga and the N planes within the unit cell move in phase. The result again is that there is an absence of dipole moment. The B_{1l} mode, even when the small N displacement is included, is still a silent mode. The mixing of the silent modes gives rise to two new silent modes.

A second possible explanation for the existence of a dipole moment could be the lack of translational symmetry due to the existence of a surface. Clearly, the asymmetry of the atomic movements in the surface gives rise to a small dipole moment. The problem with this reasoning is that the contribution of the surface to the Raman signal is very small, even in very thin nanowires, as in this case. If the diameter of our NWs is 12 nm, the perimeter is $12 \times \pi \approx 37.7$ nm. If the bond length is around 0.15 nm, then the number of atoms along a surface

section is roughly 250. However, the area of the circle is $\pi(d/2)^2 \approx 113 \text{ nm}^2$. The number of atoms in the circle is around 5000. Thus, the contribution of the surface, as compared to the bulk, is very small, even in very-thin NWs. Because both the dipole moment and the contribution to the surface are small, we can conclude that the effect of the surface is negligible. This argument is equivalent for both B_1 modes.

A third possibility is the breakdown of the selection rules due to the lack of translational symmetry produced by an impurity. Impurity-induced Raman scattering has been studied in the past, 15 and it is obviously proportional to the impurity concentration. We also discard this option given the high-purity NWs. In heavily doped crystals, impurity-induced scattering is effective, but the peak must become very broad. However, the effect would be the same for the two B_1 modes.

A fourth possibility could be that the observed peak is due to the density of two phonon states. From our lattice dynamics calculations, we obtained the two-phonon DOS (see the Supporting Information) for both the sum and the difference of energy between the phonon branches, and in none of them does there appear a peak around the frequency of the B_{1l} mode.

However, we have a peak at 320 cm^{-1} that is only observable at resonance, i.e., it is due to the Fröhlich interaction. This means that this phonon must have, compulsorily, a dipole moment. Where does this dipole moment come from? If we look at the periodic table of the elements and consider the isotopic composition of Ga and N, we find the following data: the average atomic mass of Ga is $M_{\rm av} = 69.723(1)$ amu. As is well-known, Ga has only two stable isotopes, ${\rm Ga}^{69}$ and ${\rm Ga}^{71}$. The corresponding atomic masses are $M_{\rm Ga}^{69} = 68.925580(9)$ (60.108(9)% abundance) and $M_{\rm Ga}^{71} = 70.9247005(9)$ (39.892(9)% abundance). The B_1 mode consists of two

fluctuating dipoles in opposite directions; thus, in principle, these two dipoles cancel. However, the fact that we have two different isotopes can modify this argument. Let us neglect the movement of nitrogen in the B_{11} mode. The mode consists of two Ga atoms vibrating against each other. Let us imagine that we have a mode in which the two Ga atoms are different isotopes. The options for the vibrations are Ga⁶⁹-Ga⁶⁹, Ga⁷¹-Ga⁷¹, and Ga⁶⁹-Ga⁷¹. Because the difference between the isotopes is the existence of two additional neutrons, i.e., the atomic nuclei, no argument can conclude that the "spring" constant (bonding restoring force) between them could be different because the bond is a purely electronic attraction (actually in equilibrium with the electrostatic repulsion). However, the dipole moment is the same because the "electrical" parts are identical. Thus, the only difference between the different vibrations must be the vibrational frequency. There is one vibrational frequency corresponding to the Ga⁶⁹-Ga⁶⁹ vibration, another one for the Ga⁷¹-Ga⁷¹, and a third one for the Ga^{69} - Ga^{71} mode. This slightly different ω $(\omega_2 \pm \Delta \omega)$ of course increases the broadening of the mode not only of the B_{11} mode but of all modes. However, consider the dipoles formed by N (at rest) and Ga^{71} , vibrating at a frequency ω_1 , and the dipole in the opposite direction formed with N (at rest) and Ga^{69} . Because they vibrate at a slightly different frequency, they do not cancel but instead produce a

$$p_1 \cos \omega_1 t - p_2 \cos \omega_2 t \approx 2 \sin \omega_1 t \sin \left(\frac{\Delta \omega}{2} t\right)$$

where we assume that $\omega_2 \approx \omega_1$ and $\Delta \omega = \omega_2 - \omega_1$. Not only does the cancellation disappear, but also, the dipole moment Δp reaches a maximum every period of the beat. A trivial calculation gives us a beat frequency of 0.7 MHz and an influence on the broadening of the peak of 0.02 cm⁻¹. Because the abundance of both isotopes is nearly 40%-60%, the contribution due to the dipoles becomes very important. The beat is also present in some of the remaining modes, contributing basically to the broadening, but, as we have seen, the influence on the broadening is basically negligible. Although the dipole moment is small, due to the large abundance of the isotopes, most of the lattice contributes to the dipole moment. Because Fröhlich is a long-distance interaction, the mode can be observed in a high-quality crystal. Again, the high crystal quality is essential for the observation of the forbidden mode. We can check if this explanation is consistent with the absence of the B_{1h} mode in the Raman spectra. Looking again at the periodic table, N also has two stable isotopes, N14 with 14.0030740052(9) amu. and 99.632(7)% atomic abundance and N15 with 15.0001088984(9) amu and 0.368(7)% natural abundance. The small isotopic disorder in the N, responsible for the movement in the B_{1h} mode, makes the contribution due to isotopic disorder negligible. This is why the B_{1h} mode is not observed. We can also provide a general comment on the effect of isotopic disorder on the broadening. In the work of Zhang et al., 52 for which one of the authors was the internal referee, there is a careful study of the peak position and broadening of several Ge isotopes, natural Ge, and a superlattice made by $\mathrm{Ge}^{70/76}$. The broadening is very similar in all the cases, i.e., the isotopic disorder does not contribute much to the broadening, as we predicted previously.

In conclusion, we observed an additional well-defined peak at $320.4~{\rm cm}^{-1}$ in the resonant Raman spectrum of GaN

corresponding to the B_{1l} mode. The resonant interaction of the Raman scattering is demonstrated by the enhancement of the $A_1(\text{LO})$ phonon mode. We deduce that the B_{1l} mode has a small dipole moment that enhances the strength due to Fröhlich electron—phonon interaction. Defects and impurities in thin-diameter GaN nanowires (12 nm) are unfavorable due to the self-purification mechanism. The unshifted E_{2h} mode indicates that GaN NWs are free of strain and, along with other structural and optical characterization techniques, confirms the high crystalline perfection of the GaN NWs. In summary, the high crystalline quality of the nanowires and the appearance of a small dipole moment due to isotopic disorder makes the B_{1l} silent mode appear as a Raman-allowed mode due to Fröhlich electron—phonon interaction.

The results presented here for high-quality GaN narrow NWs,can be extrapolated to other highly crystalline polar materials, such as ZnO (Zn has five stable isotopes, but 3 of them have 49, 28, and 19% natural abundances). This is not the case for InP because natural In is composed of 95% In¹¹⁵. In any case, and probably in all cases, the wire diameter must be very narrow to have both an effective self-purification effect and crystalline quality.

ASSOCIATED CONTENT

S Supporting Information

The Supporting Information is available free of charge on the ACS Publications website at DOI: 10.1021/acs.nanolett.8b01955.

Figures and details showing dispersion relations, density of states, and Raman analysis. (PDF)

AUTHOR INFORMATION

Corresponding Author

*E-mail: andres.cantarero@uv.es.

ORCID ®

Carlos Rodríguez-Fernández: 0000-0001-9024-9042 Mohammed Almokhtar: 0000-0001-8772-1553 Wilfredo Ibarra-Hernández: 0000-0002-5045-4575 Mauricio Morais de Lima, Jr.: 0000-0003-0008-6302

Aldo H. Romero: 0000-0001-5968-0571 Hajime Asahi: 0000-0002-2605-8572 Andrés Cantarero: 0000-0003-1999-4933

Author Contributions

The manuscript was written through contributions of all authors. All authors have given approval to the final version of the manuscript. All authors contributed equally to the work.

Notes

The authors declare no competing financial interest.

ACKNOWLEDGMENTS

We thank the "Dirección General de Investigación Cientifica y Técnica" for financial support through grant nos. MAT2015-63955-R and MAT2016-82015-REDT. C.R.F. thankt the FPI Programme of the Ministry of Education for young researchers. This work used the Extreme Science and Engineering Discovery Environment (XSEDE), which is supported by National Science Foundation (NSF) grant no. OCI-1053575. Additionally, the authors acknowledge the support from the Texas Advanced Computer Center (TACC) and the Bridges supercomputer at Pittsburgh Supercomputer Center. A.H.R. and W.I.H. acknowledge the support from the NSF DMREF-

NSF 1434897 and OAC-1740111 from NSF(USA) and DE-SC0016176 from the department of energy (USA). Finally, we thank the Red Española de Supercomputación for the use of the supercomputer Tirant.

REFERENCES

- (1) de Souza Schiaber, Z.; Calabrese, G.; Kong, X.; Trampert, A.; Jenichen, B.; Dias da Silva, J. H.; Geelhaar, L.; Brandt, O.; Fernández-Garrido, S. Polarity-Induced Selective Area Epitaxy of GaN Nanowires. *Nano Lett.* **2017**, *17*, 63–70.
- (2) Wahl, U.; Amorim, L. M.; Augustyns, V.; Costa, A.; David-Bosne, E.; Lima, T. A. L.; Lippertz, G.; Correia, J. G.; da Silva, M. R.; Kappers, M. J.; Temst, K.; Vantomme, A.; Pereira, L. M. C. Lattice Location of Mg in GaN: A Fresh Look at Doping Limitations. *Phys. Rev. Lett.* **2017**, *118*, 095501.
- (3) Huang, P.; Zong, H.; Shi, J.-j.; Zhang, M.; Jiang, X.-h.; Zhong, H.-x.; Ding, Y.-m.; He, Y.-p.; Lu, J.; Hu, X.-d. Origin of 3.45 eV Emission Line and Yellow Luminescence Band in GaN Nanowires: Surface Microwire and Defect. ACS Nano 2015, 9, 9276–9283.
- (4) Auf der Maur, M.; Pecchia, A.; Penazzi, G.; Rodrigues, W.; Di Carlo, A. Efficiency Drop in Green InGaN/GaN Light Emitting Diodes: The Role of Random Alloy Fluctuations. *Phys. Rev. Lett.* **2016**, *116*, 027401.
- (5) Minary-Jolandan, M.; Bernal, R. A.; Kuljanishvili, I.; Parpoil, V.; Espinosa, H. D. Individual GaN Nanowires Exhibit Strong Piezoelectricity in 3D. *Nano Lett.* **2012**, *12*, 970–976.
- (6) Watson, J.; Castro, G. A review of high-temperature electronics technology and applications. *J. Mater. Sci.: Mater. Electron.* **2015**, 26, 9226–9235.
- (7) Li, C.; Wright, J. B.; Liu, S.; Lu, P.; Figiel, J. J.; Leung, B.; Chow, W. W.; Brener, I.; Koleske, D. D.; Luk, T.-S.; Feezell, D. F.; Brueck, S. R. J.; Wang, G. T. Nonpolar InGaN/GaN Core—Shell Single Nanowire Lasers. *Nano Lett.* **2017**, *17*, 1049—1055.
- (8) Dalpian, G. M.; Chelikowsky, J. R. Self-Purification in Semiconductor Nanocrystals. *Phys. Rev. Lett.* **2006**, *96*, 226802–4.
- (9) Hugues, M.; Shields, P. A.; Sacconi, F.; Mexis, M.; Maur, M. A. D.; Cooke, M.; Dineen, M.; Di Carlo, A.; Allsopp, D. W. E.; Zúñiga Pérez, J. Strain evolution in GaN nanowires: From free-surface objects to coalesced templates. *J. Appl. Phys.* **2013**, *114*, 084307.
- (10) Cantarero, A. In *Encyclopedia of Nanotechnology*; Bhushan, B., Ed.; Springer Netherlands: Dordrecht, Germany, 2012; pp 1969–1981.
- (11) Trommer, R.; Cardona, M. Resonant Raman scattering in GaAs. Phys. Rev. B: Condens. Matter Mater. Phys. 1978, 17, 1865—1876
- (12) Möller, M.; de Lima, M. M.; Cantarero, A.; Dacal, L. C. O.; Madureira, J. R.; Iikawa, F.; Chiaramonte, T.; Cotta, M. A. Polarized and resonant Raman spectroscopy on single InAs nanowires. *Phys. Rev. B: Condens. Matter Mater. Phys.* **2011**, 84, 085318—8.
- (13) Trallero-Giner, C.; Cantarero, A.; Cardona, M. One-phonon resonant Raman scattering: Froehlich exciton-phonon interaction. *Phys. Rev. B: Condens. Matter Mater. Phys.* **1989**, 40, 4030–4036.
- (14) Ruf, T.; Phillips, R. T.; Cantarero, A.; Ambrazeviius, G.; Cardona, M.; Schmitz, J.; Rössler, U. Resonant Raman scattering and piezo-modulated reflectivity of InP in high magnetic fields. *Phys. Rev. B: Condens. Matter Mater. Phys.* **1989**, *39*, 13378–13388.
- (15) Trallero-Giner, C.; Cantarero, A.; Cardona, M.; Mora, M. Impurity-induced resonant Raman scattering. *Phys. Rev. B: Condens. Matter Mater. Phys.* **1992**, 45, 6601.
- (16) Tiginyanu, I.; Sarua, A.; Irmer, G.; Monecke, J.; Hubbard, S.; Pavlidis, D.; Valiaev, V. Fröhlich modes in GaN columnar nanostructures. *Phys. Rev. B: Condens. Matter Mater. Phys.* **2001**, *64*, 233317–3.
- (17) Sahoo, P.; Dhara, S.; Dash, S.; Tyagi, a. K.; Raj, B. Surface optical modes in GaN nanowires. *Int. J. Nanotechnology* **2010**, 9–12, 823–832.

(18) Demangeot, F.; Gleize, J.; Frandon, J.; Renucci, M. A.; Kuball, M.; Peyrade, D.; Manin-Ferlazzo, L.; Chen, Y.; Grandjean, N. Raman scattering in GaN pillar arrays. *J. Appl. Phys.* **2002**, *91*, 2866.

- (19) Kroumova, E.; Aroyo, M.; Perez-Mato, J.; Kirov, A.; Capillas, C.; Ivantchev, S.; Won- dratschek, H. Bilbao Crystallographic Server: Useful Databases and Tools for Phase-Transition Studies. *Phase Transitions* **2003**, *76*, 155–170.
- (20) Filippidis, L.; Siegle, H.; Hoffmann, a.; Thomsen, C. Hyper-Raman scattering on GaN and CdS. *Phys. Status Solidi B* **1999**, 212, R1–R2.
- (21) Hushur, A.; Manghnani, M. H.; Narayan, J. Raman studies of GaN/sapphire thin film heterostructures. *J. Appl. Phys.* **2009**, *106*, 054317
- (22) Ruf, T.; Serrano, J.; Cardona, M.; Pavone, P.; Pabst, M.; Krisch, M.; D' Astuto, M.; Suski, T.; Grzegory, I.; Leszczynski, M. Phonon Dispersion Curves in Wurtzite- Structure GaN Determined by Inelastic X-Ray Scattering. *Phys. Rev. Lett.* **2001**, *86*, 906–909.
- (23) Limmer, W.; Ritter, W.; Sauer, R.; Mensching, B.; Liu, C.; Rauschenbach, B. Raman scattering in ion-implanted GaN. *Appl. Phys. Lett.* **1998**, 72, 2589.
- (24) Harima, H. Properties of GaN and related compounds studied by means of Raman scattering. *J. Phys.: Condens. Matter* **2002**, *14*, R967–R993.
- (25) Davydov, V. Y.; Kitaev, Y. E.; Goncharuk, I. N.; Smirnov, A. N.; Graul, J.; Semchinova, O.; Uffmann, D.; Smirnov, M. B.; Mirgorodsky, A. P.; Evarestov, R. A. Phonon dispersion and Raman scattering in hexagonal GaN and AlN. *Phys. Rev. B: Condens. Matter Mater. Phys.* 1998, 58, 12899–12907.
- (26) Wiecha, P. R.; Cuche, A.; Arbouet, A.; Girard, C.; Colas des Francs, G.; Lecestre, A.; Larrieu, G.; Fournel, F.; Larrey, V.; Baron, T.; Paillard, V. Strongly directional scattering from dielectric nanowires. *ACS Photonics* **2017**, *4*, 2036–2046.
- (27) Yu, P.; Zhang, F.; Li, Z.; Zhong, Z.; Govorov, A.; Fu, L.; Tan, H.; Jagadish, C.; Wang, Z. Giant optical pathlength enhancement in plasmonic thin film solar cells using core-shell nanoparticles. *J. Phys. D: Appl. Phys.* **2018**, *51*, 295106.
- (28) Sangeetha, P.; Jeganathan, K.; Ramakrishnan, V. Micro-Raman investigations in InN-GaN core-shell nanowires on Si(111) substrates. *AIP Adv.* **2013**, *3*, 062114.
- (29) Feng, Z. C.; Wang, W.; Chua, S. J.; Zhang, P. X.; Williams, K. P. J.; Pitt, G. D. Raman scattering properties of GaN thin films grown on sapphire under visible and ultraviolet excitation. *J. Raman Spectrosc.* **2001**, *32*, 840–846.
- (30) Kuball, M. Raman spectroscopy of GaN, AlGaN and AlN for process and growth monitoring/control. *Surf. Interface Anal.* **2001**, *31*, 987–999.
- (31) Wieser, N.; Ambacher, O.; Angerer, H.; Dimitrov, R.; Stutzmann, M.; Stritzker, B.; Lindner, J. K. N. Disorder-Activated Scattering and Two-Mode Behavior in Raman Spectra of Isotopic GaN and AlGaN. *Phys. Status Solidi B* **1999**, *216*, 807–811.
- (32) Katsikini, M.; Papagelis, K.; Paloura, E. C.; Ves, S. Raman study of Mg, Si, O, and N implanted GaN. J. Appl. Phys. 2003, 94, 4389.
- (33) Wang, L. S.; Tripathy, S.; Sun, W. H.; Chua, S. Micro-Raman spectroscopy of Si-, C-, Mg- and Be-implanted GaN layers. *J. Raman Spectrosc.* **2004**, *35*, 73.
- (34) Cuscó, R.; Artús, L.; Pastor, D.; Naranjo, F. B.; Calleja, E. Local vibrational modes of H complexes in Mg-doped GaN grown by molecular beam epitaxy. *Appl. Phys. Lett.* **2004**, *84*, 897.
- (35) Rodríguez-Fernández, C.; Manzano, C. V.; Romero, A. H.; Martín, J.; Martín- González, M.; de Lima, M. M., Jr; Cantarero, A. The fingerprint of Te-rich and stoichiometric Bi2Te3 nanowires by Raman spectroscopy. *Nanotechnology* **2016**, *27*, 075706.
- (36) Almokhtar, M.; Emura, S.; Koide, A.; Fujikawa, T.; Asahi, H. Photoluminescence related to Gd3+:N-vacancy complex in GaN:Gd multi-quantum wells. *J. Alloys Compd.* **2015**, *628*, 401–406.
- (37) Almokhtar, M.; Emura, S.; Zhou, Y. K.; Hasegawa, S.; Asahi, H. Photoluminescence from *exciton*-polarons in GaGdN/AlGaN multiquantum wells. *J. Phys.: Condens. Matter* **2011**, *23*, 325802–4.

(38) Almokhtar, M.; Emura, S.; Zhou, Y. K.; Hasegawa, S.; Asahi, H. Structural, magnetic and optical studies of ultrathin GaGdN/AlGaN multiquantum well structure. *Phys. Stat. Sol.* (c) **2012**, *9*, 737–740.

- (39) Almokhtar, M.; Emura, S.; Tambo, H.; Hasegawa, S.; Asahi, H. Structural and Optical Characterization of GaN/AlGaN Single Quantum Disk Nanorods. *Acta Phys. Pol., A* **2013**, 123, 473–475.
- (40) Yu, P.; Wu, J.; Liu, S. T.; Xiong, J.; Jagadish, C.; Wang, Z. M. Design and fabrication of silicon nanowires towards efficient solar cells. *Nano Today* **2016**, *11*, 704–737.
- (41) Chèze, C.; Geelhaar, L.; Brandt, O.; Weber, W. M.; Riechert, H.; Münch, S.; Rothemund, R.; Reitzenstein, S.; Forchel, A.; Kehagias, T.; Komninou, P.; Dimitrakopulos, G. P.; Karakostas, T. Direct comparison of catalyst-free and catalyst-induced GaN nanowires. *Nano Res.* **2010**, *3*, 528–536.
- (42) Hohenberg, P.; Kohn, W. Inhomogeneous Electron Gas. *Phys. Rev.* **1964**, *136*, B864–B871.
- (43) Kohn, W.; Sham, L. J. Self-Consistent Equations Including Exchange and Correlation Effects. *Phys. Rev.* **1965**, *140*, A1133–A1138.
- (44) Ibarra-Hernandez, W.; Elsayed, H.; Romero, A. H.; Bautista-Hernandez, A.; Olguín, D.; Cantarero, A. *Phys. Rev. B: Condens. Matter Mater. Phys.* **2017**, *96*, 035201.
- (45) Gonze, X. Adiabatic density-functional perturbation theory. Phys. Rev. A: At., Mol., Opt. Phys. 1995, 52, 1096–1114.
- (46) Gonze, X.; et al. Recent developments in the ABINIT software package. Comput. Phys. Commun. 2016, 205, 106.
- (47) Gonze, X.; et al. ABINIT: First-principles approach to material and nanosystem properties. *Comput. Phys. Commun.* **2009**, *180*, 2582–2615.
- (48) Gonze, X.; et al. A brief introduction to the ABINIT software package. Z. Kristallogr. Cryst. Mater. 2005, 220, 558–562.
- (49) Perdew, J. P.; Burke, K.; Ernzerhof, M. Generalized Gradient Approximation Made Simple. *Phys. Rev. Lett.* **1996**, *77*, 3865–3868.
- (50) Perdew, J. P.; Burke, K.; Ernzerhof, M. Generalized Gradient Approximation Made Simple [Phys. Rev. Lett. 77, 3865 (1996)]. Phys. Rev. Lett. 1997, 78, 1396–1396.
- (51) Olguin, D.; Cantarero, A.; Cardona, M. Electron-phonon effects on the direct band gap in semiconductors: LCAO calculations. *Solid State Commun.* **2002**, *122*, 575–589.
- (52) Zhang, J. M.; Giehler, M.; Göbel, A.; Ruf, T.; Cardona, M.; Haller, E. E.; Itoh, K. Phys. Rev. B: Condens. Matter Mater. Phys. 1998, 57, 1348.